JOURNAL OF MATERIALS SCIENCE 18 (1983) 2923–2938

Chemically-assisted fracture of thermoplastic PET reinforced with short E-glass fibre*

CHANG LHYMN, J. M. SCHULTZ
Center for Composite Materials, University of Delaware, Newark, Delaware 19711, USA

The study of the stress–rupture lifetime of a PET/glass fibre system by means of fracture mechanics methods indicates the degradation of lifetime under an aggressive environment (10% HCl solution). The SEM–EDAX analysis reveals the depletion of calcium and aluminium elements from the fibre, and this is believed to be the cause of multiple fibre fractures. The fracture toughness is decreased because the role of fibre pull-out, which is the significant energy-consuming process, is negligible. A statistical analysis, from which the lifetime behaviour can be predicted, is carried out.

1. Introduction

The corrosion resistance of a fibre-reinforced plastic (FRP) is important when applied under an aggressive environment. Generally, FRP is superior to metals or alloys in resisting corrosive attack, but it is known that FRP's can be weakened under an aggressive environment [1–3]. In composites, the weak spot is either a glass fibre or an interface [4–6]. In this context the polymeric matrix protects the weak spots. If the weak spots are somehow exposed to a corrosive medium by diffusive flow of chemicals or by microcracks, then corrosion of the fibre and the interface can occur.

In this study, the fracture mechanics approach originally developed for metallic materials [7] is applied to investigate the corrosion behaviour of a short fibre composite under an acidic solution during constant load rupture testing. Microscopy examinations are also reported. Previous tests under various acidic solutions [6] indicate that most attack occurs at the fibre/matrix interfaces and at the fibres, while the matrix is insensitive to the aggressive medium. The ultimate cause of deterioration was not quite clear, and the lifetime behaviour was not quantitatively explained. This paper addresses the above two questions.

2. Experimental procedures

The experimental details are given elsewhere [8, 9]. The test material is a thermoplastic poly(ethylene terepthalate) (PET) matrix, specifically formulated for rapid crystallization during injection moulding, dispersed with short E-glass fibres. The weight fraction of fibres is 45% and the fibre diameter is about 10 μm. Recently, it was discovered that in the kind of short-fibre-reinforced thermoplastic sheets used in this study (Rynite® 545), the fibre orientation varies systematically across the specimen thickness [8, 9]. The authors showed that near the mould surface the fibres are aligned in the mould-fill direction (MFD), while the centre section, away from the surface, contained fibres which lay preferentially normal to both the specimen thickness and the MFD. A cross-sectional micrograph across the thickness direction of a sheet plaque of 1/16 inch thickness is shown in Fig. 1.

The geometry of compact tension specimens is shown in Fig. 2, as reported elsewhere [9]. Three kinds of machine-notch geometry are used; T-specimen ($\theta = 90^\circ$), 45°-specimen ($\theta = 45^\circ$), and L-specimen ($\theta = 0^\circ$). Here, θ denotes the angle between the MFD and the notch.

The aggressive chemical used is a 10% solution of HCl in water. Every specimen was pre-soaked in 10% HCl solution for one week prior to testing. The actual testing was done with the specimen immersed in the HCl solution. A scanning electron microscope (SEM) was used to observe the fractured surface, and the compositional profile was

*Supported under the University–Industry Research Program of the Center for Composite Materials at the University of Delaware.

0022–2461/83 $03.00 + .12

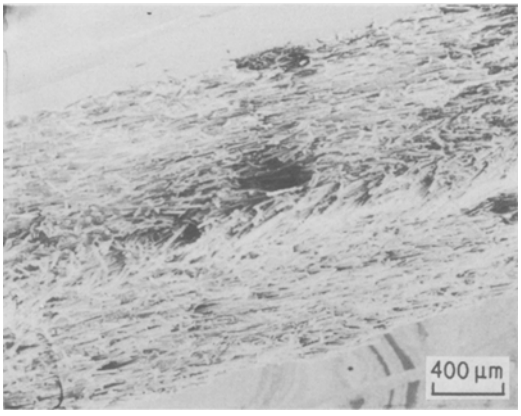

Figure 1 Cross-sectional view of 1/16 inch as-moulded Rynite® through the thickness direction.

determined by the energy-dispersive X-ray analysis (EDAX) system attached to the SEM. Since the actual probing of the fibre exposed to the HCl solution during stress-rupture testing is very difficult, the flat specimen was simply immersed in a 10% HCl solution for a specified time period and then probed. In this way, the effect of HCl solution on the fibre composition could be determined and be compared to the initial uncorroded specimen, eliminating the stress factor in a stress corrosion test. Fig. 3 illustrates the sequence of this corrosion test. For reference, the average fibre length is about 200 μm.

3. Results and discussion

3.1. Effect on chemical corrosion

The compositional profiles (EDAX analysis) are shown in Figs. 4 and 5 for both corrosion and virgin (no acid treatment) specimens respectively. Both specimens are flat to maintain the same take-off angle (between the specimen surface and the direction of the measured X-rays). The probed mode automatically makes the highest peak (silicon) full-scale at all times by continuously renormalizing the display.

By taking the relative ratio of aluminium/silicon and calcium/silicon of both corrosion and initial specimens, it is clear that the aluminium and calcium elements are relatively depleted in the case of the corrosion sample. The local depletion of aluminium and calcium could cause a local pitting, which acts as a stress-raiser for the eventual fibre cracking as observed in the actual stress-corrosion test shown in Fig. 6. Therefore, the compositional variation based on an ideal flat specimen under a corrosive medium indicates indirectly the cause of multiple fibre fracture events along the crack path. It is believed that the leached-out calcium and aluminium elements remain in an ionized state in solution. The sequence of events is visualized in Fig. 7.

Fig. 6 illustrates the fibre surface exposed to a HCl solution, revealing numerous fibre fractures and interfacial cracking. The matrix fracture as well as fibre fracture seem to suggest that the cracking may be due to the internal stresses.

3.2. Fractography

The SEM observation of fibres and matrix was also fruitful. The morphological features of the frac-

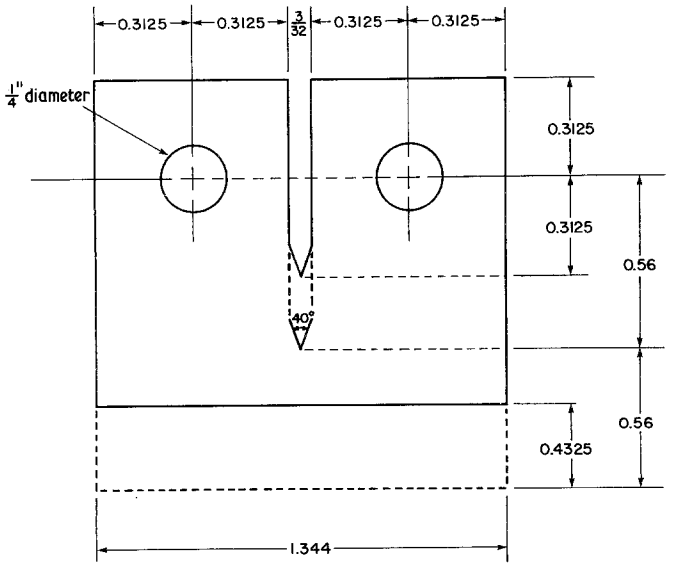

Figure 2 Geometry of compact tension specimen.

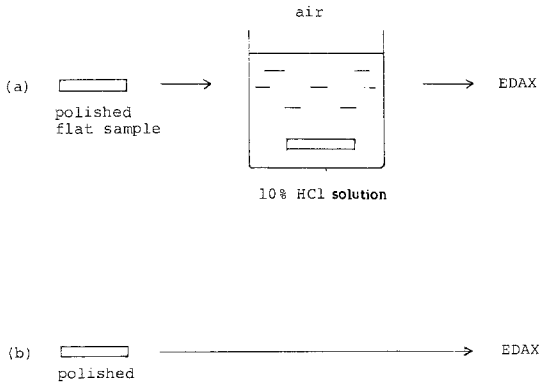

Figure 3 Corrosion experiment for EDAX analysis: (a) corroded, and (b) uncorroded.

ture surface are revealed in Figs. 8 and 9. Structurally speaking, two things are different from the case of uncorroded fracture:

1. White dots observed under SEM on a two-dimensional surface are a charging effect caused by the formation of micropits or microcracks (see Fig. 8).

2. Numerous fibre fractures in a fibre are seen, both of macroscopic and microscopic nature (Fig. 9).

The depletion of calcium and aluminium in a fibre produces an open structure, which is less resistant to chemical attack than the initial structure. Perhaps even more importantly, the local pitting produces stress-raisers. Bond scission is easily accomplished at a region of local stress enhancement during slow propagation of the crack front. The end result is the microcracking of a fibre at various locations along its length (Figs. 8

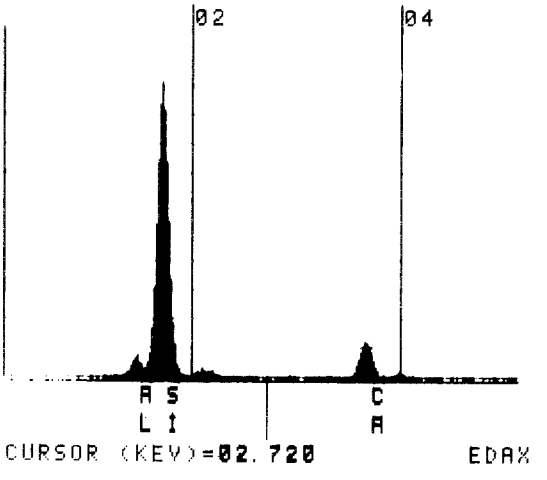

Figure 4 EDAX profile of corroded specimen.

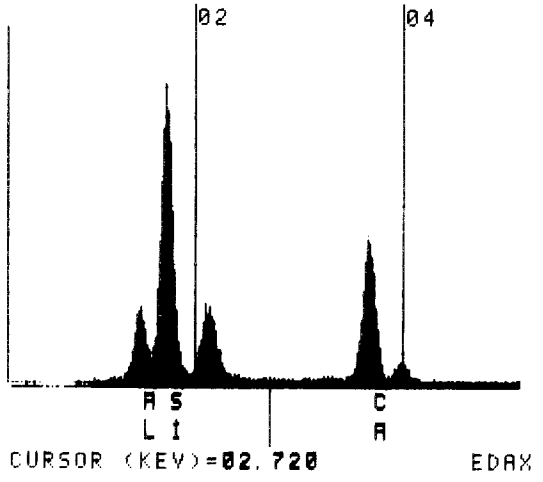

Figure 5 EDAX profile of uncorroded (air) specimen.

and 9). The model of chemically-assisted fracture is given in Fig. 7.

Fibres are thus easily fractured around the crack tip due to the combined action of stress concentration and chemical attack. Easy fibre fracture on the crack front means that fibre pull-out (which was abundant in the static rupture case under an air environment) does not occur, and therefore the fracture plane is quite flat (Fig. 10a). Figs. 10a to d are a series of micrographs from the same sample along the crack path. The area near the notch, where the crack papagates slowly (Figs. 10a and b), is very flat. The area near the other end of the specimen, where the crack propagates almost instantaneously, shows a lot of fibre pull-out and a ragged fracture surface. This is shown in Figs. 10c and d.

The implication of the elimination of the fibre pull-out process for fracture is that the energy of

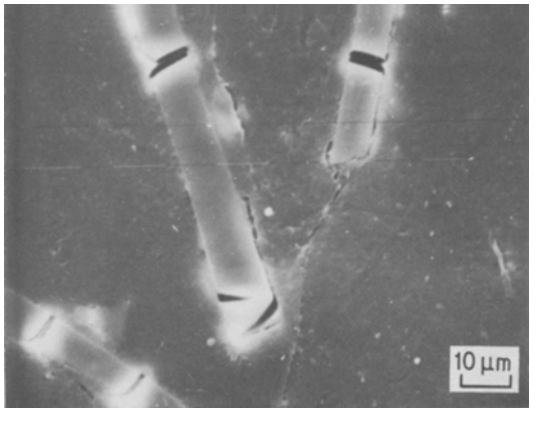

Figure 6 Surface micrograph of corroded specimen.

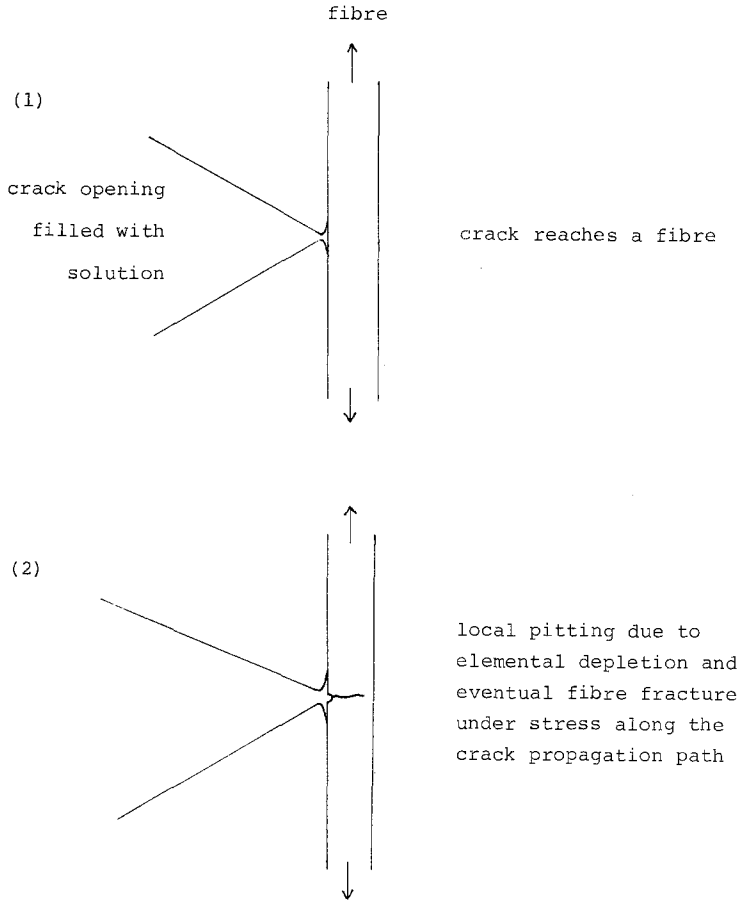

Figure 7 Fibre cracking at the crack tip under an aggressive environment.

fracture is reduced, eventually lowering the fracture toughness as will be shown in the next section.

Initially, the crack propagates slowly at an area near the notch tip. During this stage, the fibre is weakened by the penetration of a corrosive fluid and thus the fracture plane is flat. At an area remote from the notch tip, the crack propagates rapidly and significant penetration and attack by the aggressive medium does not take place. Therefore, at this remote area, the fracture surface is very ragged and shows a lot of fibre pull-out. This expected change in the fractographic aspect is verified in Figs. 11a and b, which are taken of the same specimen.

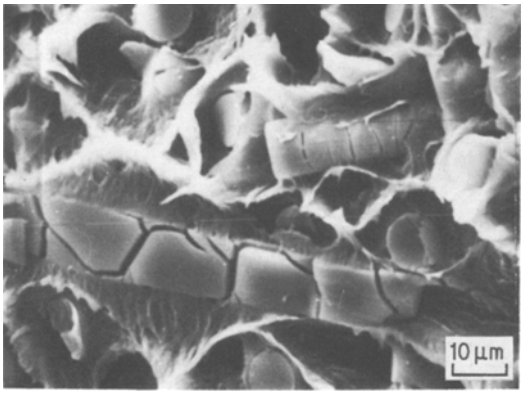

Figure 8 SEM view of corroded 45°-specimen after failure.

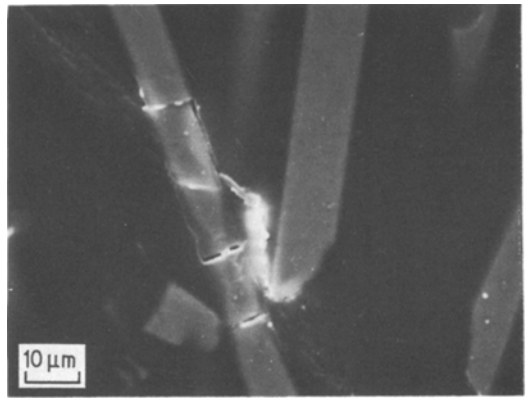

Figure 9 Two-dimensional micrograph under a stage of crack propagation.

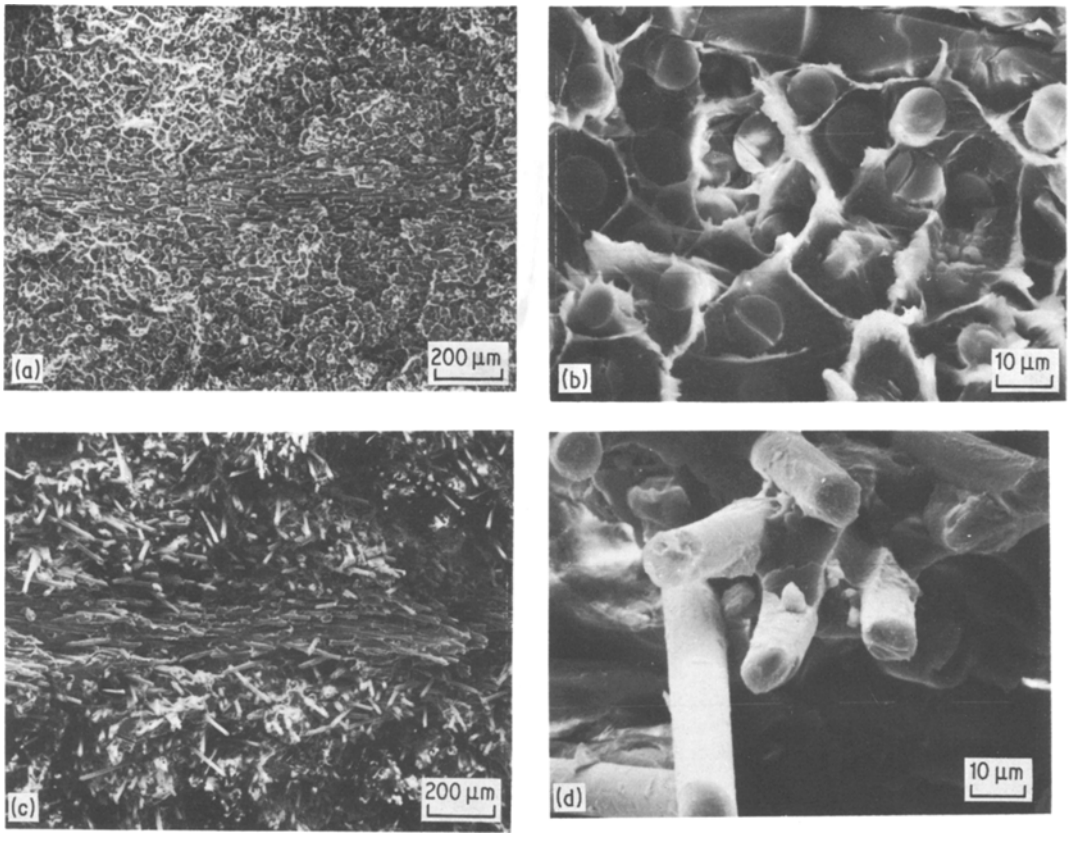

Figure 10 (a) Fracture plane near the notch area of a natural 1/16 inch laminate. (b) T-configuration section of (a). (c) Fracture plane of the zone of fast crack propagation. (d) Magnified area of (c).

Generally, matrix cracking starts from the fibre ends in radial direction. Neighbouring cracks (preceded by a crazing process) from adjacent fibre ends meet together to form a yielded zone and shear rupture (see Fig. 11b).

When the duration of stress-corrosion is not long enough, a mixed mode of matrix fracture (ductile and brittle) is seen, as in Fig. 12. Here, in the zone of brittle fracture, the interface has not yet deteriorated and the fibre is still intact. Such an interface-dominated fracture area is brittle. When the critical interfacial shear stress is greater

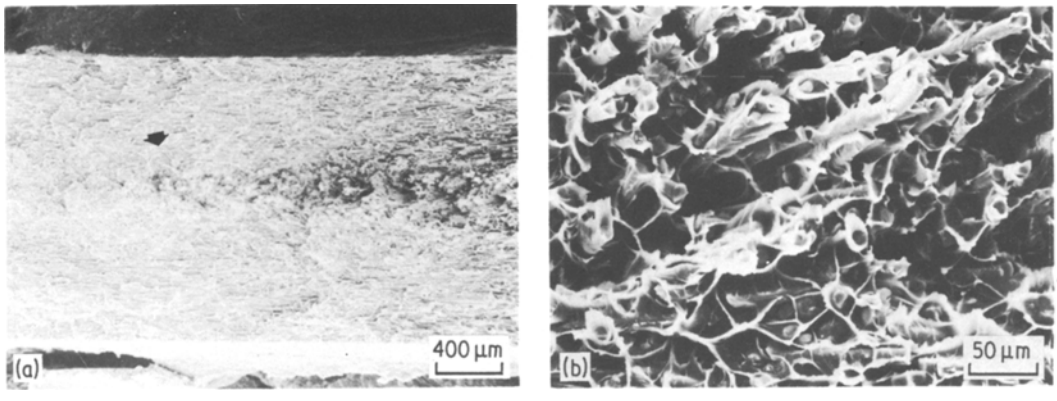

Figure 11 Stress corrosion fracture plane of (1/16 inch) LTL natural laminate, showing a transitional mode of core T region from the notch (left) to the specimen end. Fibre pull-out begins to show up at the arrow point. (b) Transitional area of (a).

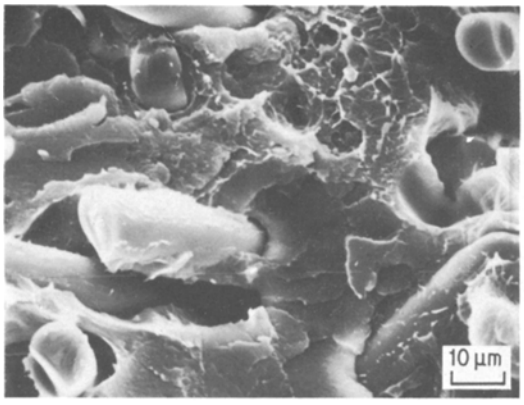

Figure 12 Notch area of a fractured specimen which has been pre-soaked in a 10% HCl for 48 h.

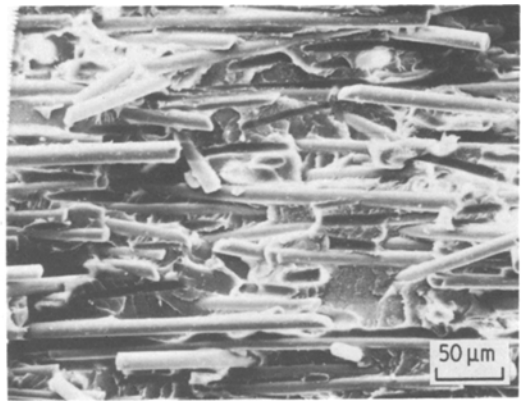

Figure 14 SEM view of an area remote from the notch of the 45°-specimen.

than the matrix yield strength, the matrix starts to fail before interfacial bonding occurs. This seems to be the case of cohesive debonding. When the crack propagates quickly, the fibres are not so weakened, due to there being insufficient time for chemical attack. In this case, the shear stress along the fibre/matrix interface is lower than the normal stress required for fibre fracture at the crack front. The end result is a fibre pull-out under high speed crack propagation (Fig. 11b).

The chemically-assisted fracture of 45° specimens reveals two regions of crack propagation: slow propagation during the intial stage of crack growth and fast propagation during the later stage of crack instability. During the period of slow propagation, fibre fractures are induced so that the crack propagates along the direction perpendicular to the stress axis (Fig. 13).

In this region near the notch, the material fails in a ductile mode. In a region remote from the machine-notch, the crack propagates quickly and the material fails in a brittle mode as shown in Fig. 14. It is clear that the brittle failure occurs mainly along the fibre/matrix interface and along the matrix phase connecting the discrete interfaces (Fig. 14). In a region of ductile failure (Fig. 13), numerous fibre fractures are seen as well as interface and matrix fracture. The macroscopic fracture path in a brittle region is roughly at 45° to the stress axis, while fracture in a ductile region occurs roughly at 90° to the tensile axis, initially due to the occurrence of numerous fibre crackings. As shown before, the fibre fracture in this stress corrosion test is the result of chemical attack and thus such a chemical attack requires a certain incubation time (acid penetration and reaction). This time is available in a region of ductile failure where the crack propagates slowly, but is not available in a region of brittle failure where the crack propagates quickly.

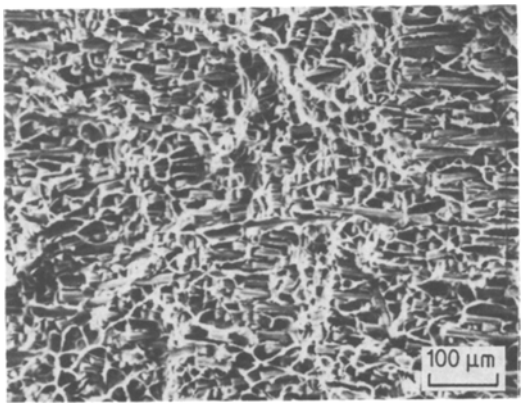

Figure 13 Area near notch of 45°-specimen.

The crack growth of a T-specimen under stress corrosion is shown in Figs. 15a and b. Fibre fracture under an air environment is induced by a far-field effect, away from the immediate crack front. The crack front does not directly cause fibre fracture but provides additional energy for crack propagation along the fibre/matrix interface. Fibre fracture under an aggressive environment is induced by both far-field and by the local crack front. When the crack front approaches a fibre, the chemical attack weakens the fibre section exposed to a corrosive fluid. The dominance of fibre fracture instead of interface fracture (and subsequent fibre pull-out) causes a relatively quite planar fracture mode.

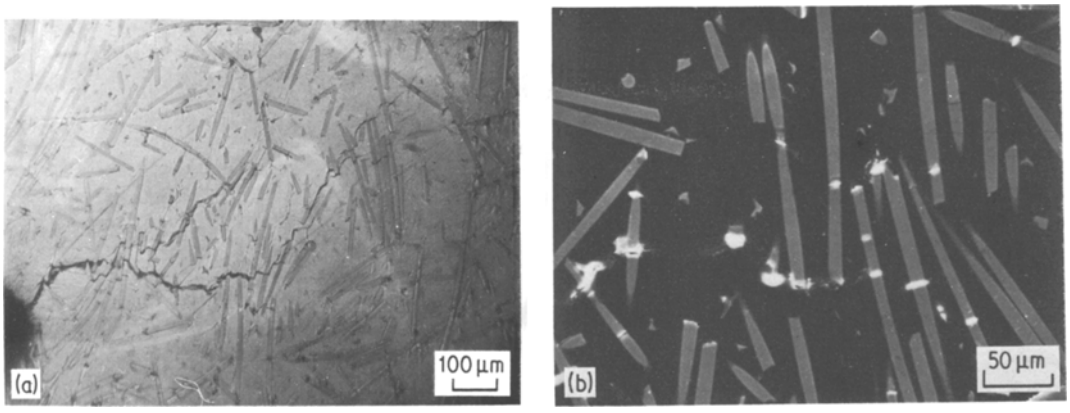

Figure 15 Stress-corroded crack propagation for T-specimen.

3.3. Stress-rupture lifetime

The stress intensity factor equation for a compact tension specimen can be presented in the form [10]:

$$K_c = \frac{P}{Ba^{1/2}} f\left(\frac{a}{w}\right) \quad (1)$$

where P is the applied load, B is the specimen thickness, and $f(a/w)$ is a geometrical correlation factor. K_c is defined as the value of the stress intensity factor K_I at which a crack in the specimen begins to grow unstably. Such a K_c is of a macroscopic nature, based on a homogeneous and isotropic material. The lifetime data for various specimens under an air and 10% HCl solution environment are shown in Figs. 16 and 17 respectively. The specimens are as-moulded "natural" laminate of three layers (LTL or TLT). The K_c plotted is the initial stress intensity factor. The air-failure case shows a very weak (almost time-independent) slope, while the 10% HCl-failure case reveals a reduced lifetime effect for long-time stress-rupture tests. The reduction of lifetime in the case of stress-corrosion is due to fibre deterioration, reducing the role of fibre pull-out in fracture toughness. These qualitative aspects will be quantified by statistical modelling in a later section.

3.4. Static failure criteria

From the previous sections, the following facts are established:

1. There is a ductile-to-brittle transiton in the fracture mode of stress-ruptured specimens. The ductile zone near the notch area is where the crack grows slowly, in a step-wise fashion [9].

2. The lifetime data (time-to-failure, t_F against K_c) indicates that there is a lower bound limit of K_{scc}, below which the specimen never fractures ($t_F \to \infty$) for materials tested in air. Instantaneous fracture is characterized by zero t_F and this is the upper bound limit of initial K_c.

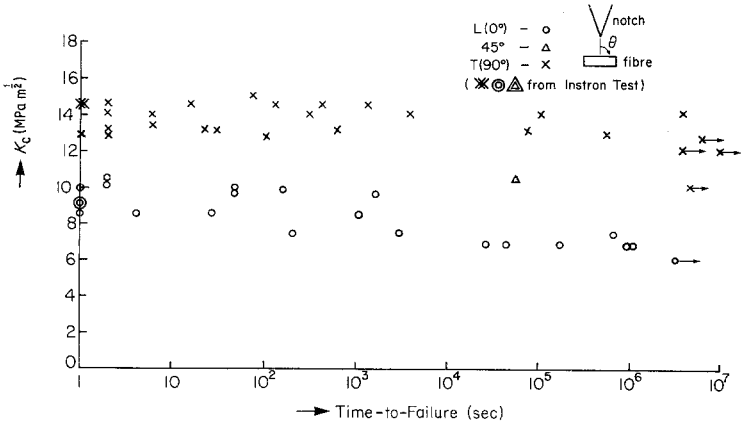

Figure 16 Lifetime (t_F) against K_1 data of triple layer specimens under an air environment.

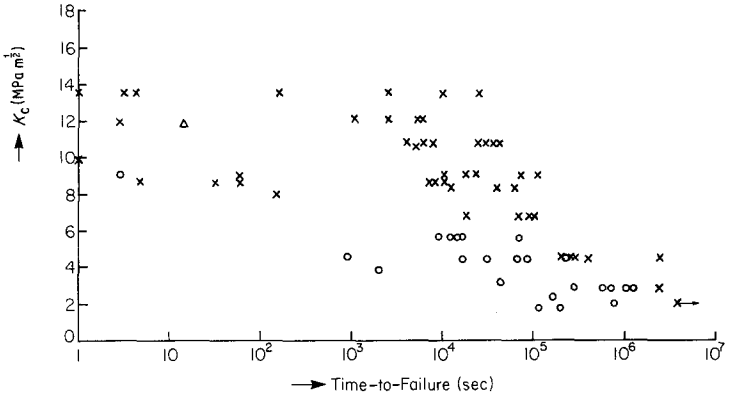

Figure 17 t_F against K_1 data for stress-corrosion test of triple layer specimens.

3. Between these two bounds, the K_c–t_F data show a wide scatter, with a very weak slope.

The critical length concept is introduced to explain the above facts.

The crack growth behaviour can be generalized as shown in Fig. 18, where the interfacial and matrix fracture are identified. The sequential growth process is transformed to a velocity (v)–time (t) graph and then finally to an average velocity ($\bar{v}$)–time-to-failure (t_F) shape. Each process is assumed to have a characteristic crack growth velocity and the δ-function-like fibre fracture event away from the advancing crack tip is not shown

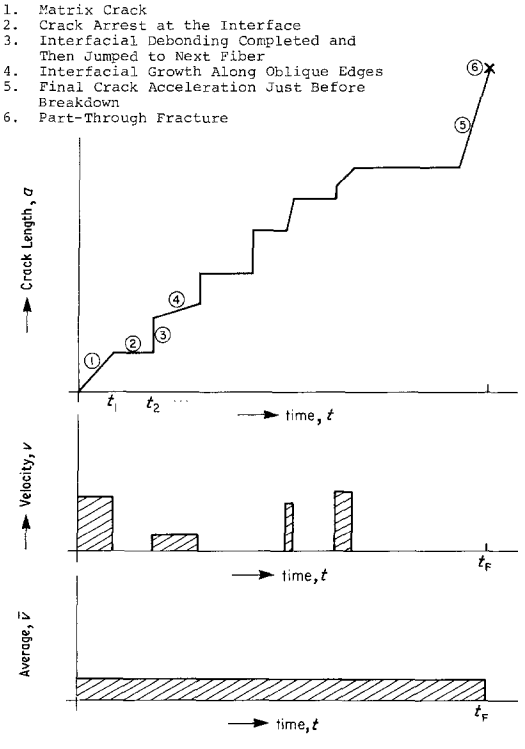

Figure 18 Crack growth and its equivalent transformation.

but is assumed to be integrated to the final $\bar{v}$–t_F rectangle. Mathematically,

$$\sum_i (v_i \Delta t_i)_{\text{at } x_i} = (\bar{v}) t_F \tag{2}$$

where x_i is the location of the cracking event.

In order for a part-through breakdown, the area ($\bar{v}t_F$) is assumed to be greater than a certain critical value L^*, i.e.

$$\bar{v} t_F \geqslant L^* \tag{3}$$

Experimental evidence seems to indicate that the onset of sudden breakdown is related to the transition (from ductile to brittle) behaviour in the case of sustained load cracking. Consequently, it is reasonable to assume that L^* is nearly equal to the length L_d of the ductile zone.

$$L^* \simeq + L_d \tag{4}$$

Here, L^* is the integrated length while the so-called plastic zone size is an instantaneous zone near the crack tip and has no bearing on the sudden breakdown.

Presumably L_d grows with the time of sustained loading and somehow depends on the load:

$$L_d = K(P) t \tag{5}$$

where $K(P)$ is a load-dependent constant.

The actual observation of stress-rupture data indicates three kinds of crack length–time behaviour (Fig. 19). Guided by the above phenomena, it is assumed that Fig. 20 is the functional form of $K(P)$ for different orientations. From the relation

$$t_F = \frac{L^*}{K(P)} \tag{6}$$

we can understand the instantaneous breakdown ($t_F = 0$) and apparent crack arrest ($t_F = \infty$).

The branchy aspect of crack propagation mani-

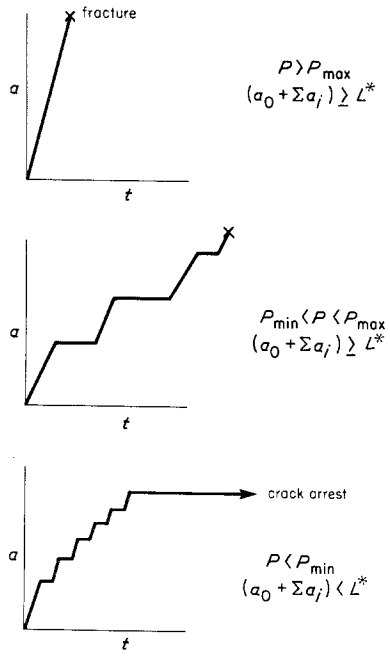

Figure 19 Three modes of crack growth behaviour.

fested at various locations, included in the summation over i in Equation 2, induces a relaxation of stress concentration at the crack tip as well as the randomness of the crack path, particularly for a T-specimen. The localized processes, indicated by the summation over i, are precursors of crack

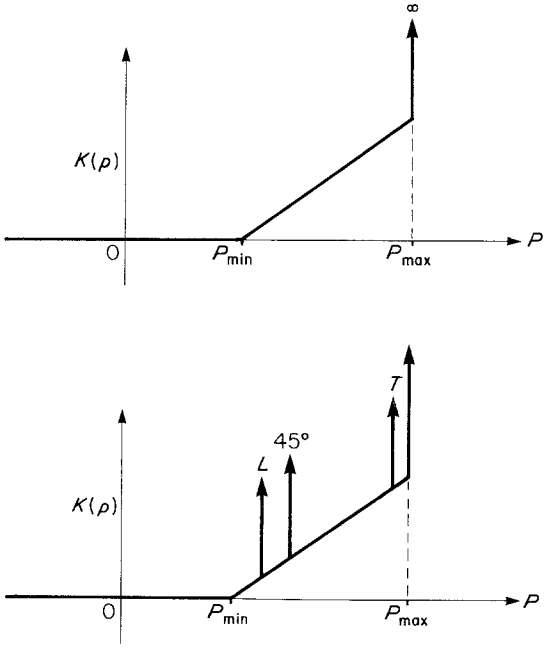

Figure 20 $K(p)$ dependence on the orientation of fibre.

connectivity through weak channels. So, this critical length model contains the far-field effect as its starting point.

The concept of fracture mechanics is applicable in the L^* representation. At the moment of reaching L^*, the stress concentration at the main crack tip reaches a critical value to cause catastrophic failure. Also, note the introduction of lower and upper bounds on $K(P)$.

$L^* = K(P)t$ where $K(P)$ may be of several forms; linear, parabolic, exponential, etc. $K(P)$ can be regarded as a measure of velocity and classically the velocity $da/dt = \alpha K_1^n$, where α and n are material constants and K_1 the mode I stress intensity factor [11]. Thus,

$$L^* = \alpha K_1^n t = \alpha \left[\frac{P}{WB^{1/2}} f\left(\frac{a}{w}\right)\right]^n t \qquad (7)$$

Therefore, the material property $K(P)$ comes from two constants α and n and the value of n determines the shape of $K(P)$ between the lower and upper bounds.

For a specific material two bounds, P_{min} and P_{max}, are determined from the stress-rupture tests. The $K(P)$ form is experimentally deduced from the measurements of L^* for specific P and t values. From this $K(P)$ curve the material constants α and n could be obtained by approximation.

3.5. Statistical analysis

The actual measurement of the length, L, of the ductile zone is given in Fig. 21. It can be safely assumed that L^* = constant. So, $\alpha K_1^n t$ = constant. This is equivalent to $CK_1^n = 1$, where C is equal to (α/constant). So, the critical length concept naturally arrives at the lifetime model.

As can be perceived from Figs. 16 and 17, the lifetime data is not deterministic but statistical. For each stress level, the scatter in the lifetime can be fitted to a certain distribution function. The Weibull distribution is particularly useful as a model for product life, having a great variety of shapes which can be extremeley flexible in the fitting of data. Thus, the approach to the K_1–t_f characterization is based on the previous lifetime model and a Weibull distribution of time-to-failure. The details of the Weibull distribution is given in the Appendix.

Applying the model proposed by Whitney [12] for the static rupture case, the distribution of lifetimes at a specific stress level can be expressed by the two-parameter Weibull distribution function,

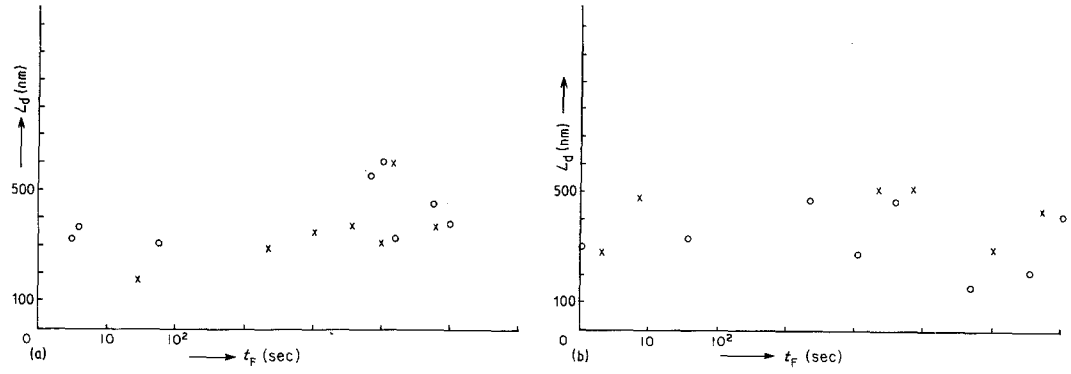

Figure 21 L_d against t_F data of (a) triple layer specimens, and (b) single layer specimens.

$$R(t_F) = \exp\left[-\left(\frac{t_F}{t_0}\right)^{\alpha_f}\right] \quad (8)$$

where $R(t_F)$ denotes the reliability of t_F (the probability of survival), t_0 is the characteristic time-to-failure (the "location parameter"), and α_f is the "shape parameter".

From $CK_I^b t_F = 1$ and $R(t_F) = \exp[-(t_F/t_0)^{\alpha_F}]$

$$K_I = A\left\{\left[-\ln R(t_F)\right]\frac{1}{\alpha+b}\right\} t_F - \frac{1}{b} \quad (9)$$

where $A \equiv C^{(-1/b)}$. Since $-\ln R(t_0) = 1$, the following equation is easily derived:

$$K_I(t_0) = A t_0^{(-1/b)} \quad (10)$$

Therefore, a plot of $\log K_I$ against $\log t_0$ produces a straight line with slope $(-1/b)$ and a y-intercept of $\log A$.

The K_I–t_F curve for any reliability can be produced in the following way. Using $t_0 = C^{-1}K_I^{-b}$, one writes

$$R(t_F) = \exp\left[-\left(\frac{t_f}{C^{-1}K_I^{-b}}\right)^{\alpha_f}\right] \quad (11)$$

Solving for K_I,

$$K_I = A\{[-\ln R(t_F)]^{(1/\alpha_f b)}\}t_F^{(1/b)} \quad (12)$$

The stress-corrosion data of single layer specimens (prepared by machining off the upper two layers) are shown in Fig. 22. It is clear that the initial K_c value required for part-through failure is lower in the case of stress-corrosion for long-time rupture. The stress-corrosion for fibre fracture requires a certain time to leach out some elements, so that the reduced lifetime effect due to weakened fibres is seen for long-time stress-rupture tests.

The spread of lifetime data points in a single layer tends to merge together in a natural three-layer laminate, probably due to the averaging effect of multi-layers.

In order to obtain the unknown parameters (α_f, b, A) the data reduction scheme is chosen: (a) fitting the t_f data at each stress range to a two-parameter Weibull distribution; (b) determination of α_f by a data pooling technique; (c) fitting $\ln K_I$ against $\ln t_0$ data to a straight line to determine b and A.

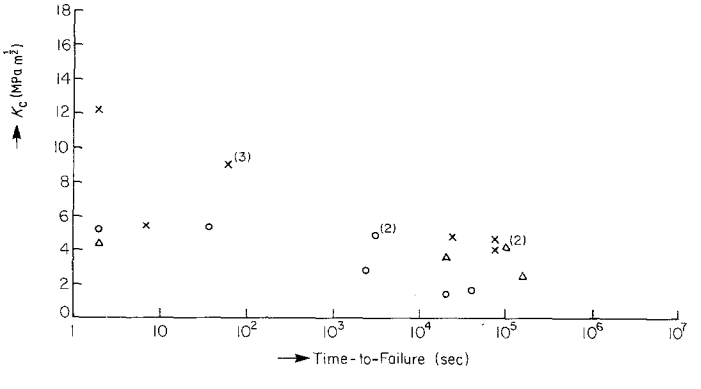

Figure 22 Chemically-assisted fracture lifetime data for specimens of single layer.

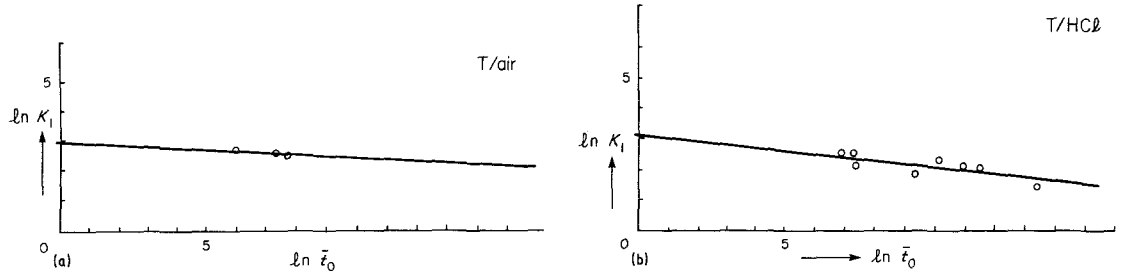

Figure 23 $\ln K_1$ against $\ln t_0$ data for (a) (T/air) specimens, and (b) (T/HCl) specimens.

When the number of specimens tested at the ith stress level, K_i, is denoted as n_i, and m is the number of stress levels tested, the following data set is obtained.

$$N_i(N_{i1}, N_{i2}, \ldots, N_{in_i}),\ i = 1, 2, \ldots, m$$

As shown in detail in the Appendix, the maximum likelihood estimate (MLE) method is used to determine α_{fi} and t_{0i}.

$$\frac{\sum_{j=1}^{n_i} (t_{ij})^{\hat{\alpha}_{fi}} (\ln t_{ij})}{\sum_{j=1}^{n_i} (t_{ij})^{\hat{\alpha}_{fi}}} - \frac{1}{n_i} \sum_{j=1}^{n_i} t_{ij} - \frac{1}{\hat{\alpha}_{fi}} = 0 \quad (13)$$

$$t_{0i} = \frac{1}{n_i} \left(\sum (t_{ij})^{\hat{\alpha}_{fi}} \right) \frac{1}{\hat{\alpha}_{fi}} \quad (14)$$

where $\hat{\alpha}_{fi}$ and $\hat{t}_{0i}$ denote estimated values of α_{fi} and t_{0i}. The iterative analysis is used to obtain a value of $\hat{\alpha}_{fi}$ to any desired accuracy [13]. Here n_i is the number of test specimens tested at the ith stress level.

A single value of $\bar{\alpha}_f$ for all K_1 levels is determined by a data pooling technique [14]. Utilizing the normalized data set

$$X_{ij} = \frac{t_{ij}}{t_{0i}} \quad (15)$$

each set of data at a given stress (K_{1i}) range is normalized by the characteristic time-to-failure and the results are fitted to the pooled two-parameter Weibull distribution

$$R(x) = \exp\left[-\left(\frac{x}{x_0} \right)^{\bar{\alpha}_f} \right] \quad (16)$$

For pooled parameters, the MLE procedure produces the following α_f values:

$$(\alpha_f)_{T/HCl} = 0.616$$

$$(\alpha_f)_{L/HCl} = 0.622$$

$$(\alpha_f)_{T/air} = 0.291$$

$$(\alpha_f)_{L/air} = 0.389$$

Here, a high α_f implies a narrow spread of lifetime data.

The values of $\hat{t}_{0i}$ are adjusted by the equation $\bar{t}_{0i} = \bar{x}_0 \hat{t}_{0i}$, where $\bar{t}_{0i}$ is the estimated value of t_0 associated with the adjusted two-parameter Weibull distribution, $R(x) = \exp(-x^{\alpha_f})$. Here, the location parameter, x_0, is adjusted to be unity for a perfect fit to the data pooling scheme.

From the data of the $\log K_1$ against $\log t_{0i}$ curve (Figs. 23 and 24), the least squares fitting procedure produces

$$(b)_{T/HCl} = 10$$

$$(b)_{L/HCl} = 19.2$$

$$(b)_{T/air} = 29.1$$

$$(b)_{L/air} = 21.8$$

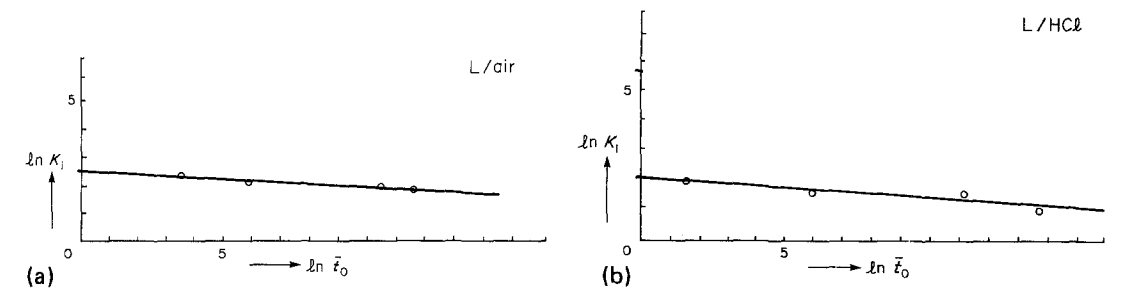

Figure 24 $\ln K_1$ against $\ln t_0$ data of (a) (L/air) specimens, and (b) (L/HCl) specimens.

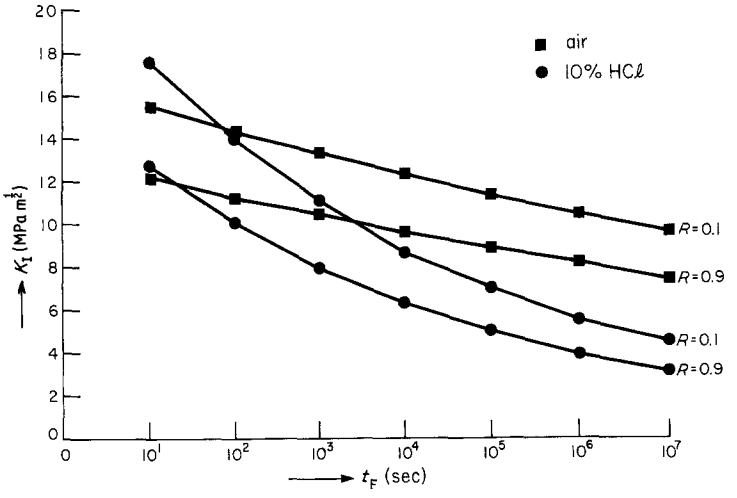

Figure 25 Lifetime prediction model of T-specimens.

and from the intercept

$$(A)_{T/HCl} = 22.87$$

$$(A)_{L/HCl} = 7.39$$

$$(A)_{T/air} = 17.28$$

$$(A)_{L/air} = 11.58$$

So, the lifetime prediction model becomes

$$(K_1)_{T/HCl} = 22.89\left[(-\ln R)\frac{1}{0.6.6 \times 10}\right]t_F^{(-1/10)} \quad (17)$$

for a certain reliability R.

Likewise,

$$(K_1)_{L/HCl} = 7.39\left[(-\ln R)\frac{1}{0.622 \times 19.2}\right]t_F^{(-1/19.2)} \quad (18)$$

$$(K_1)_{T/air} = 17.28\left[(-\ln R)\frac{1}{0.291 \times 29.1}\right]t_F^{(-1/29.1)} \quad (19)$$

$$(K_1)_{L/air} = 11.58\left[(-\ln R)\frac{1}{0.389 \times 21.8}\right]t_F^{(-1/21.8)} \quad (20)$$

The result of one calculation is shown in Figs. 25 and 26 for reliabilities $R = 0.1$ and 0.9 as examples. For a specific K_1 value, the dominating failure mode corresponds to the shortest lifetime (t_F) mode.

Since the material constant in the power law equation of lifetime behaviour are derived from the preliminary experimental data, the final results of Figs. 25 and 26 must reflect the experimental observations. As expected, the lifetime follows the air-rupture case initially, but when the fibre is weakened by a compositional depletion after a cer-

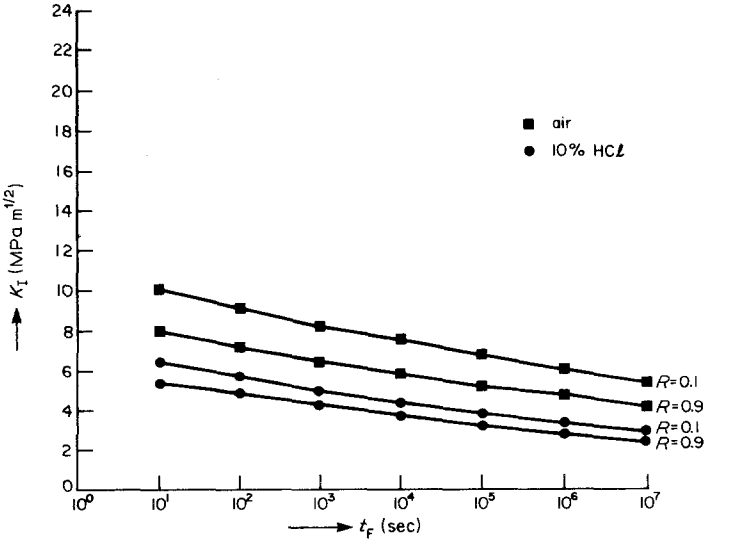

Figure 26 Lifetime prediction model of L-specimens.

tain time period, the lifetime switches to the acid-rupture case. When the fracture process is dominated by fibre, the lifetime data shows an almost time-independent behaviour, but when the fibre is sufficiently weakened, the fracture mode changes into the matrix-dominating one. The degree of fitting of lifetime data to the two-parameter Weibull distribution function is shown in the Appendix.

4. Conclusions

The "critical barrier" model of lifetime prediction is well aligned with the experimental data, since it is based on solid assumptions derived from fractographic observations. The relatively small number of tests is enough to determine two material constants.

The aluminium and calcium content of the fibre is decreased during stress-corrosion and the subsequent pit formation (or the tensile stress induced by volume change) is the precursor of massive fibre cracking of stress-corroded specimens.

Acknowledgements

The authors are grateful to Drs E. Deyrup and B. Epstein of the Du Pont Company for supplying injection moulded Rynite® plaques, for useful consultation, and for their generous support of this work.

We acknowledge also the work and patience of the office and artistic staff of the Center for Composite Materials. We are indebted also to Professor R. B. Pipes for his support of this program. Finally, we are grateful to J. Quigley who provided the existing Fortran programs for MLE calculation.

Appendix

Method of maximum likelihood [13]

For a continuous distribution, the likelihood $L(\theta)$ for a complete sample of n observations $x_1, x_2, \ldots, x_n$ is defined as the joint probability density, i.e. $L(\theta) = f(x_1; \theta)x, \ldots, xf(x_n; \theta) = \Pi_{i=1}^{n} f(x_n; \theta)$, where θ is an unknown parameter and $f(x; \theta)$ is a probability density function. For a discrete distribution, the probability mass function is used in place of the probability density, i.e. $L(\theta) = \Pi_{i=1}^{n} P(x_i; \theta)$, where $P(x_i; \theta)$ is a probability mass function. The maximum likelihood estimator (MLE) of θ, say θ, is the value of θ that maximizes L or the logarithm of L. The MLE of θ is a solution of $\mathrm{d}(\log L)/\mathrm{d}\theta = 0$.

The Weibull distribution [13]

The Weibull probability density function having two-parameters is

$$f(t) = \frac{\alpha}{t_0}\left(\frac{t}{t_0}\right)^{(\alpha-1)} \exp[-(t/t_0)^{\alpha}] \quad \text{(A1)}$$

The parameter t_0, often called the characteristic life, is a scale parameter specifying the 63.2th distribution percentile and determines the spread. The parameter α, known as the shape parameter, determines the shape of the distribution and is positive. Analytical estimates of the two parameters should in general be obtained iteratively, and very often the method of maximum likelihood is used.

For a sample of size n, the likelihood function $L = f(t_1, \ldots, t_r)$ can be expressed

$$L = \frac{n!}{(n-r)!}\prod_{i=1}^{r}\left\{\frac{\alpha}{t_0}(t_i/t_0)^{(\alpha-1)}\exp[-(t_i/t_0)^{\alpha}]\right\} \times (1-\{1-\exp[-(t_s/t_0)^{\alpha}]\})^{(n-r)} \quad \text{(A2)}$$

where $t_s = t_e$ (a specified test termination time) for Type 1 censoring and $t_s = t_{(r)}$ (the observed time of the rth failure) for Type 2 censoring, at which time testing is terminated. From the conditions of $\partial(\ln L)/\partial t_0 = 0$ and $\partial(\ln L)/\partial\alpha = 0$, the following forms are obtained:

$$\frac{\sum_{i=1}^{r}(t_i)^{\alpha}\ln t_i + (n-r)(t_s)^{\alpha}\ln t_s}{\sum_{i=1}^{r}(t_i)^{\alpha} + (n-r)t_s^{\alpha}} - \frac{1}{\alpha} - \frac{1}{r}\sum_{i=1}^{r}\ln t_i = 0 \quad \text{(A3)}$$

and

$$t_0^{\alpha} = \frac{1}{r}\left[\sum t_i^{\alpha} + (n-r)t_s^{\alpha}\right] \quad \text{(A4)}$$

Since $n = r$ and $\alpha = \alpha_f$ in the present case, Equations 13 and 14 can be obtained. For reference, the Weibull reliability function for the proportion surviving an age of at least t_f is

$$R(t_f) = \exp[-(t_f/t_0)^{\alpha}], t_f > 0 \quad \text{(A5)}$$

Generally, the reliability function $R(t)$ for a life distribution is

$$R(t) = \int_t^{\infty} f(t)\,\mathrm{d}t = 1 - F(t) \quad \text{(A6)}$$

where $f(t)$ is a probability density, and $F(t)$ is the cumulative distribution function with a probability density $f(t)$:

$$F(t) = \int_{-\infty}^{t} f(u)\,\mathrm{d}u \quad \text{(A7)}$$

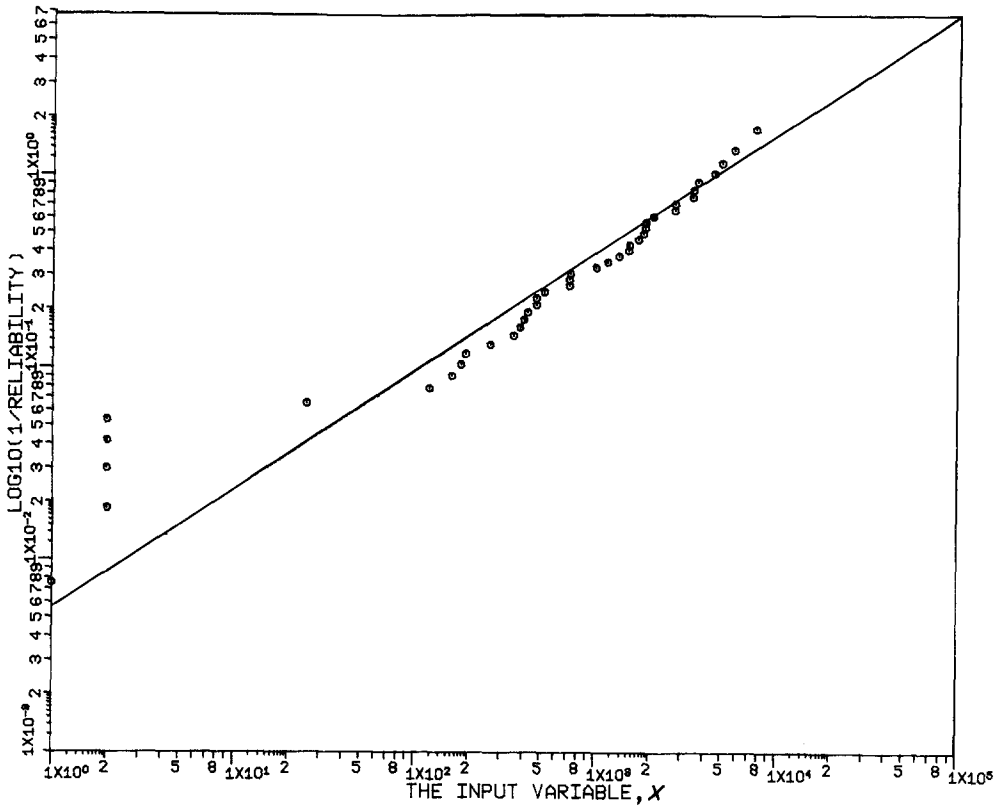

Figure A1 Comparison between data and two-parameter Weibull distribution for (T/HCl) specimens. $\hat{\alpha}_f = 0.616$.

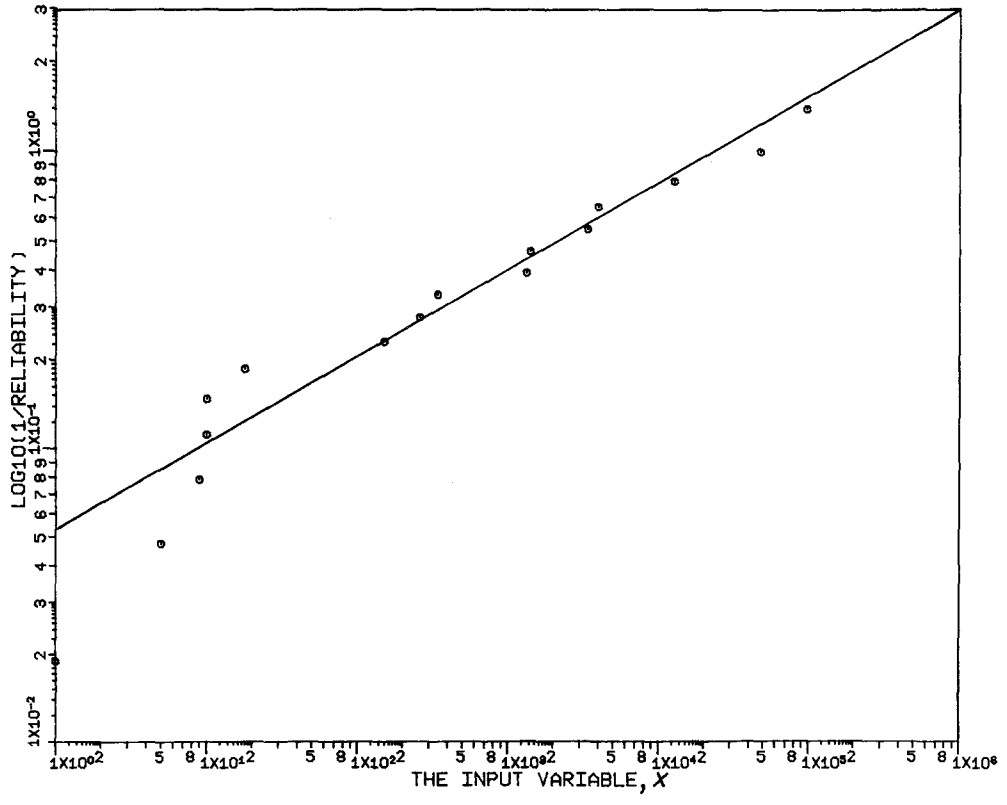

Figure A2 Comparison between data and Weibull distribution for (T/air) specimens. $\hat{\alpha}_f = 0.29$.

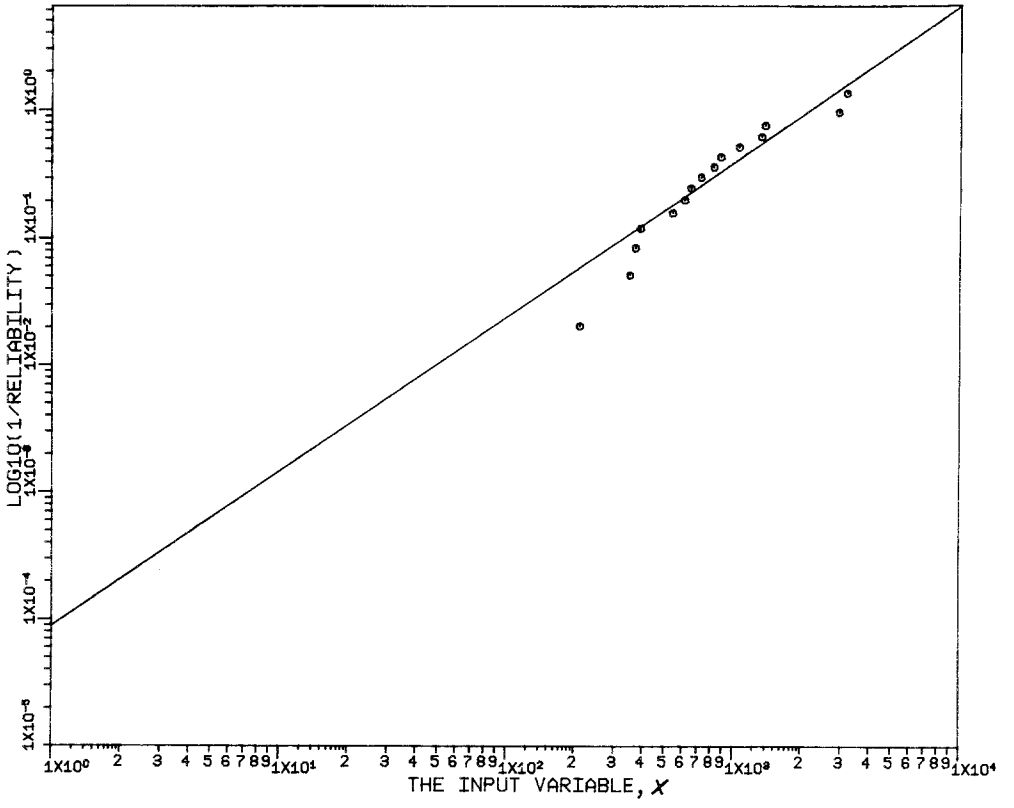

Figure A3 Comparison between data and Weibull distribution for (L/HCl) specimens. $\bar{\alpha}_f = 1.22$.

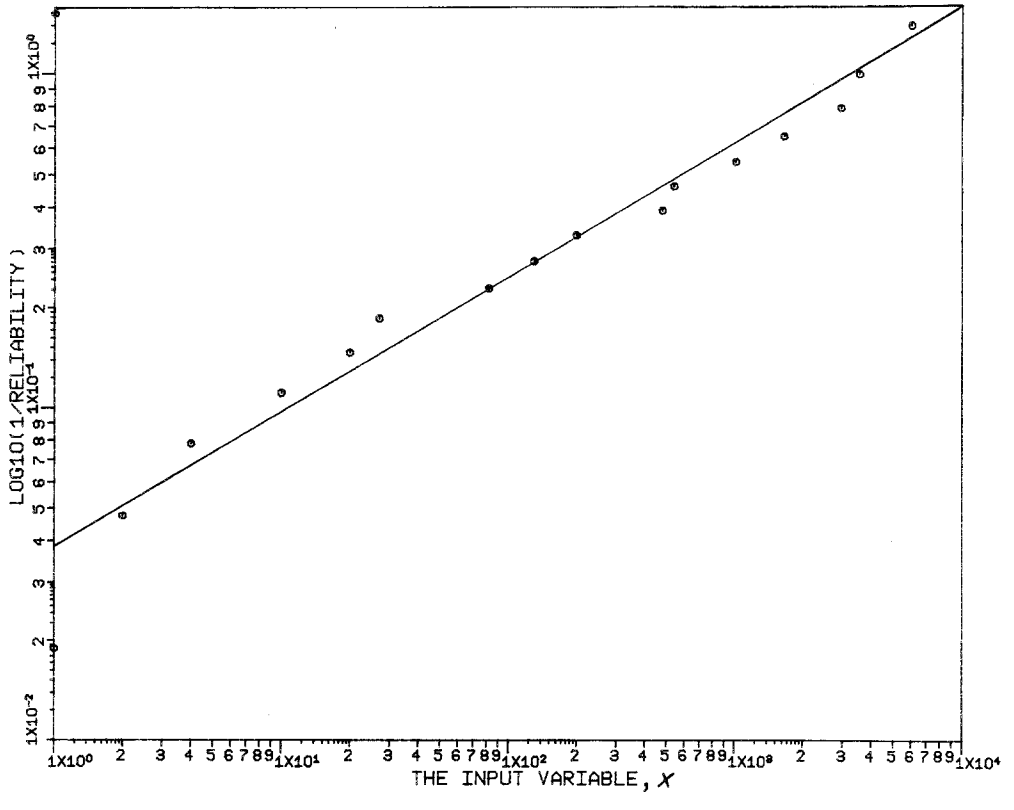

Figure A4 Comparison between data and Weibull distribution for (L/air) specimens. $\bar{\alpha}_f = 0.389$.

For the Weibull probability density function $f(t)$,

$$F(t) = 1 - \exp[-(t/t_0)^{\alpha}], \quad t > 0 \quad \text{(A8)}$$

$$R(t) = \exp[-(t/t_0)^{\alpha}], \quad t > 0 \quad \text{(A9)}$$

Data fitting

The data pooling technique compares the Weibull distribution and the data as shown in Figs. A1, A2, A3 and A4, respectively for T/HCl, T/air, L/HCl and L/air cases. Here the input variable is given by

$$x \equiv \left(\frac{t_{ij}}{t_{0i}}\right) \times 10^3. \quad \text{(A10)}$$

References

1. R. C. ALLEN, *Polym. Eng. Sci.* **19** (1979) 329.
2. J. AVESTON, Proceedings of the 3rd International conference on composite materials, Paris, 1980 (Pergamon Press, Oxford, 1980) p. 556.
3. D. HULL and P. J. HOGG, *ibid.* 543.
4. J. C. HAARSMA, Proceedings of the 34th Annual Conference on Reinforced Plastics and Composites, January 1979 (Institute of SPI, New Orleans, 1979) Paper 22-E.
5. S. TONP and R. ARVESEN, *ibid.* Paper 13-D.
6. K. FRIEDRICH, *J. Mater. Sci.* **16** (1981) 3292.
7. R. W. HERZBERG, "Deformation and Fracture Mechanics of Engineering Materials" (John WIley and Sons, New York, 1976) Chap. 8.
8. K. FRIEDRICH, CCM-80-19, Center for Composite Materials, University of Delaware (1980).
9. C. LHYMN and J. M. SCHULTZ, *J. Mater. Sci.* in press.
10. S. T. ROLFE, "Fracture and Fatigue Control in Structures" (Prentice Hall Inc., Englewood Cliffs, NJ, 1977) Chap. 3.
11. A. KELLY and L. N. McCARTREY, *Proc. Roy. Soc. Lond. A* **374** (1981) 475.
12. J. M. WHITNEY, *ASTM STP* **723** (1981) 133.
13. N. R. MANN, R. E. SCHAFER and N. D. SINGPURWALLA, "Methods for Statistical Analysis of Reliability and Life Data" (Wiley, New York, 1974) Chap. 4.
14. R. V. WOLFF and G. H. LEMON, AFML-TR-74-197, March 1976.

Received 18 October 1982
and accepted 18 February 1983